34th Annual International Conference of the IEEE EMBS
San Diego, California USA, 28 August - 1 September, 2012

Singular Spectrum Analysis Improves Analysis of Local Field Potentials from Macaque V1 in Active Fixation Task

Pietro Bonizzi, Joël Karel, Peter De Weerd, Eric Lowet, Mark Roberts,
Ronald Westra, Olivier Meste, and Ralf Peeters

Abstract— **Local field potentials (LFPs) represent the relatively slow varying components of the neural signal, and their analysis is instrumental in understanding normal brain function. To be properly analyzed, this signal needs to be separated in its fundamental frequency bands. Recent studies have shown that empirical mode decomposition (EMD) can be exploited to pre-process LFP recordings in order to achieve a proper separation. However, depending on the analyzed signal, EMD is known to generate components that may cover a too wide frequency range to be considered as narrow banded. As an alternative, we present here an improved version of the singular spectrum analysis (SSA) algorithm, validated by numerical simulations, and applied to LFP recordings in V1 of a macaque monkey exposed to simple visual stimuli. The components generated by the improved SSA algorithm are shown to be more meaningful than those generated by EMD, paving the way for its use in LFP analysis.**

I. INTRODUCTION

Given a localized area in the brain, local field potentials (LFPs) represent the relatively slow varying temporal components of the neural signal (the synchronized dendritic input) picked up from within a few hundreds of microns of a recording electrode. Superimposed on the LFP are the temporal distributions of action potentials (the output from the recorded neural population). The study of the processes underlying LFPs is considered important in understanding information transmission in the brain. For example, current technologies permit the recording of ongoing LFPs measured from different cortical layers, using depth probes with recording contacts spread along a linear recording shaft to cover the entire depth of cortex. This opens the possibility of studying information transmission across cortical layers by the analysis of coherence among different layers [1].

In vision, it is well-established that stimulation causes a relative enhancement of power within a spectral band centered in the gamma-band frequency region of 30 to 100 Hz [2], [3]. Specific theoretical proposals have pointed out the prominent role of coherence in the gamma-band range as a vehicle for communication among different neuronal populations. While the classical view of the function of coherence is that of a clock keeping excitatory and inhibitory phases of activity in communicating populations in a specific frequency and phase, gamma-band coherence has been shown recently to not require a stable frequency but to be maintained despite a shift in peak frequency governed by stimulus contrast [4].

However, a detailed time-frequency analysis of LFPs requires LFPs from distinct populations to be studied separately from population spiking. Moreover, it is necessary to focus on specific frequency bands, asking for band separation techniques. As gamma oscillations have been discovered to be nonstationary in the visual cortex [4], and EEG signal is known to be nonlinear [5], tools able to capture nonstationary and nonlinear dynamics are required. To achieve this at the level of single trials (stimulus presentations), Liang *et al.* have shown the usefulness of pre-processing univariate neurobiological time series recorded during visual attention task with empirical mode decomposition (EMD) [5]. By virtue of EMD, LFPs can be indeed resolved into a sum of intrinsic components where high-frequency components have been mainly identified with gamma-band oscillations (30-90 Hz). This decomposition allows one to achieve a meaningful Hilbert Spectrum [6], thus providing a high resolution time-frequency analysis not affected by the Heisenberg uncertainty principle, as for the standard spectrogram. Indeed, the Short Time Fourier Transform and the Wavelet Transform provide limited resolution in time and frequency [5]. Hence, EMD is expected to decompose a nonlinear and nonstationary signal in narrow band components. Additionally, these components are interpretable in terms of the signal structure, which is more difficult for wavelet coefficients. However, depending on the analyzed signal, the first obtained component may cover a too wide frequency range to be considered narrow band [7].

A method which shares common features with EMD is the singular spectrum analysis (SSA) [8]. SSA decomposes a nonlinear time series into a sum of several interpretable additive components (trend, oscillatory components, and noise). SSA has been proven useful in the analysis of EEG recordings for the identification of sleep stages [9] or the detection of seizure [10]. SSA is able to focus on narrow band components of the analyzed signal, which makes this method a suitable pre-processor of LFP recordings. Additionally, it can be used for change-point detection [11]. The only limitation is that in its standard definition, the *window length* for the analysis needs to be set by the user.

In this study, we present an improved SSA algorithm able to perform a data driven decomposition of a signal, in which the window length is automatically defined on the spectral properties of the signal. The method is validated through

P. Bonizzi, J. Karel, R. Westra, and R. Peeters are with the Dep. of Knowledge Eng., Maastricht University, Maastricht, The Netherlands. pietro.bonizzi@maastrichtuniversity.nl

P. De Weerd, E. Lowet, M. Roberts are with the Dep. of Cog. Neuroscience, Maastricht University, and with the Donders Institute, Radboud University Nijmegen, The Netherlands.

O. Meste is with the Laboratoire I3S, Sophia Antipolis, France.

numerical simulations and shown to outperform EMD in the extraction of narrow band components. Moreover, comparison with EMD is also performed on real LFP recordings from macaque V1 cortex undergoing visual stimulation task. The proposed algorithm is shown to generate gamma-band components characterized by higher energy than those given by EMD, more suitable in tracking the changes in the gamma-band energy content before and after stimulus presentation.

II. METHODS

A. EMD and SSA

EMD is a fully adaptive, data-driven approach that decomposes a nonlinear and non-stationary signal into a linear combination of intrinsic oscillatory modes, called intrinsic mode functions (IMFs) [6], [12]. The IMFs are amplitude-modulated/frequency-modulated components which can be seen as oscillations underlying the observed signal. To ensure that the time frequency spectra yield meaningful frequency estimates, IMFs are functions with symmetric upper and lower envelopes and for which the number of zero crossings and the number of extrema differ at most by one. The standard EMD algorithm decomposes a signal $y(t)$ as $y(t) = \sum_{i=1}^{F} c_i(t) + r(t)$, where $\{c_i(t)_{i=1}^{F}\}$ is the set of F IMFs, and $r(t)$ is a monotonic residue. To extract the IMFs, an iterative method known as the sifting process is used.

SSA consists of two complementary stages: *decomposition* and *reconstruction* [8]. Given a time series $x(n)$, $n = 0, \ldots, N-1$, assumed to be stationary in the weak sense, let L be an integer (window length), $1 < L < N$. The embedding procedure forms $K = N - L + 1$ lagged vectors $\mathbf{x}_i = (x(i), \ldots, x(i+L-1))^{\mathrm{T}}$, with $i = 1, \ldots, N-L+1$. The trajectory matrix of the series $x(n)$ is then given by $\mathbf{X} = [\mathbf{x}_1, \mathbf{x}_2, \ldots, \mathbf{x}_K]^{\mathrm{T}}$, such that this is a Hankel matrix (constant skew-diagonals). The singular value decomposition (SVD) of $\mathbf{X}$ is then computed, providing $\mathbf{X} = \mathbf{U}\mathbf{D}\mathbf{V}^{\mathrm{T}}$, with $\mathbf{U} = (K \times L)$ and $\mathbf{V} = (L \times L)$ containing the left and right singular vectors, respectively, and $\mathbf{D} = (L \times L)$ being the diagonal matrix containing the singular values (the square root of the corresponding eigenvalues λ). Matrix $\mathbf{X}$ is thus decomposed in a sum of rank-one matrices $\mathbf{X}_i$ such that $\mathbf{X} = \sum_{i=1}^{L} \mathbf{X}_i = \sum_{i=1}^{L} \sqrt{\lambda_i} U_i V_i^{\mathrm{T}}$. Matrix $\mathbf{X}$ is then reconstructed by exploiting $\mathbf{X}_1$ only (the largest eigenvalue and eigenvector), such that $\mathbf{X}_1 = \sqrt{\lambda_1} U_1 V_1^{\mathrm{T}}$. The last step in basic SSA transforms $\mathbf{X}_1$ into a new series of length N. Defining matrix $\mathbf{Y}$ as the $(L \times K)$ 90 degree counterclockwise rotation of matrix $\mathbf{X}_1$, diagonal averaging transfers the matrix $\mathbf{Y}$ to the series $g(n)$, $n = 0, \ldots, N-1$ by averaging each diagonal k of $\mathbf{Y}$, $diag(\mathbf{Y}, k)$ (with $k = -L-1, \ldots, N-L$), so that $g(n) = \frac{1}{L} \sum_L diag(\mathbf{Y}, n-L+1)$. The first component $g_1(n)$ is subtracted from $x(n)$, and the second component $g_2(n)$ is computed from the residual (with L unchanged).

B. Improved SSA

As underlined in Section I, the window length L is to be set before applying SSA. The final result is highly dependent on the particular choice of L and this can present an issue when a priori knowledge about the frequency-bands corresponding to the weak stationarities contained in the analyzed signal is absent. Hence, we propose the following improvement. Given the time series $x(n)$, its Fourier Transform is obtained and the dominant frequency f_D in its spectrum is identified. Hence, the window length L is set to the inverse of f_D, such that $L = \frac{1}{f_D} F_S$, where F_S is the sampling frequency. In case $f_D = 0$, L is set to $\frac{F_S}{2}$ to identify very low frequency oscillations. The first component $g_1(n)$ is then subtracted from $x(n)$, a new L is computed for the residual, and the procedure is repeated to find the second component $g_2(n)$. The algorithm is terminated when the last component does contribute to the reconstruction of the original signal for less than 0.01%.

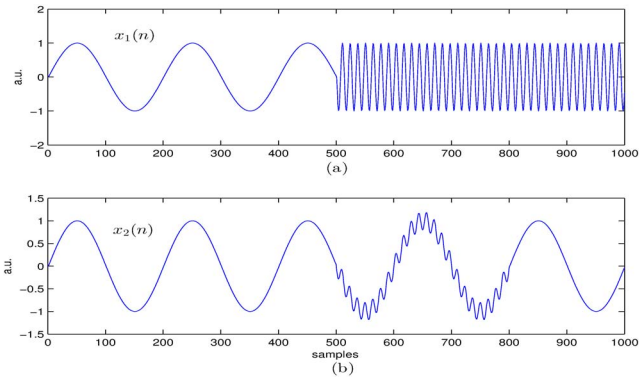

Fig. 1. (a) Signal $x_1(n)$ generated by the first simulation. (b) Signal $x_2(n)$ generated by the second simulation; a.u.: arbitrary units.

III. METHOD VALIDATION

A. Simulation Design

We define two harmonic signals characterized by dominant frequencies in different frequency-bands, such that:

$$\begin{aligned} s_1(n) &= \sin(2\pi f_1 / F_s n) \\ s_2(n) &= \sin(2\pi f_2 / F_s n) \end{aligned} \quad (1)$$

with $f_1 = 5$ Hz, $f_2 = 75$ Hz, and $F_s = 1$ kHz. In the first simulation, we considered a concatenation of the two harmonic signals $s_1(n)$ and $s_1(n)$, as follows:

$$x_1(n) = \begin{cases} s_1(n) & \text{for } n = 0, \ldots, 499 \\ s_2(n) & \text{for } n = 500, \ldots, 999 \end{cases}$$

In the second simulation, we consider the partial superposition of the low frequency harmonic signal $s_1(n)$ and a low-amplitude version of the high frequency signal $s_2(n)$, as follows:

$$x_2(n) = \begin{cases} s_1(n) & \text{for } n = 0, \ldots, 499 \\ s_1(n) + 0.2 s_2(n) & \text{for } n = 500, \ldots, 799 \\ s_1(n) & \text{for } n = 800, \ldots, 999 \end{cases}$$

Signals $x_1(n)$ and $x_2(n)$ are represented in Fig. 1-(a) and 1-(b), respectively.

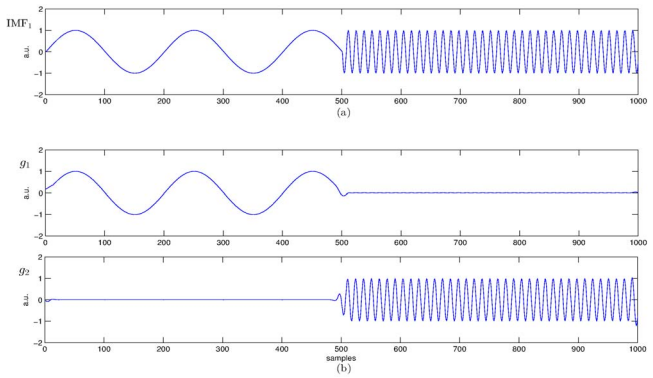

Fig. 2. (a) The IMF obtained from the EMD of the first simulated signal $x_1(n)$. (b) The two main components obtained from the SSA of the first simulated signal $x_1(n)$; a.u.: arbitrary units.

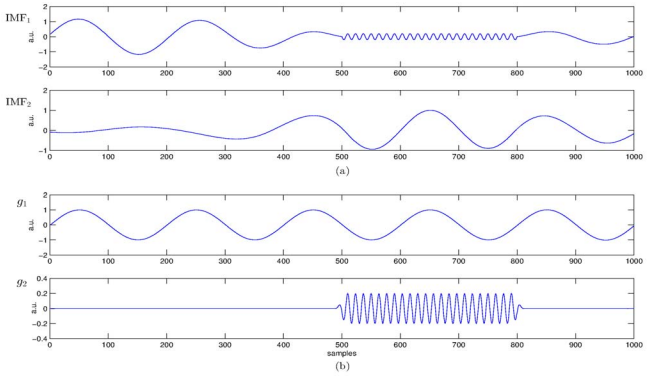

Fig. 3. (a) The first two IMFs obtained from the EMD of the second simulated signal $x_2(n)$. (b) The two main components obtained from the SSA of the second simulated signal $x_2(n)$; a.u.: arbitrary units.

B. Simulation Results

Fig. 2 reports the results obtained by applying EMD and the improved SSA to the first simulated signal, $x_1(n)$. As can be noticed from Fig. 2-(a), the application of EMD to $x_1(n)$ generates only one IMF (IMF_1), identical to the original signal. This is because signal $x_1(n)$ is built so as to satisfy the two conditions for a signal to be considered an IMF (symmetric upper and lower envelopes and identical number of zero crossings and extrema). Hence, EMD is shown to be unable to decompose $x_1(n)$ in its two main components. Conversely, the application of SSA to $x_1(n)$, as shown in Fig. 2-(b), generates two main components (g_1 and g_2), which account for 99.89% of the variance of $x_1(n)$, each one representing one of the two component in $x_1(n)$.

Fig. 3 reports the results obtained by applying EMD and the improved SSA to the second simulated signal, $x_2(n)$. It can be noticed how the first two IMFs provided by the EMD of $x_2(n)$, accounting for the 99.05% of the variance in $x_2(n)$, both contain information about the two components in $x_2(n)$ (Fig. 3-(a)), whereas SSA generates two components, accounting for the 99.96% of the variance in $x_2(n)$, each one representing one of the two harmonics composing $x_2(n)$ (Fig. 3-(b)).

Hence, SSA was able to decompose a signal in narrow-band components from two representative simulated signals, whereas EMD failed to produce an equivalent narrow-band separation. Moreover, additional simulations showed SSA to be insensitive to pink noise, a characteristic noise in the LFP power spectrum.

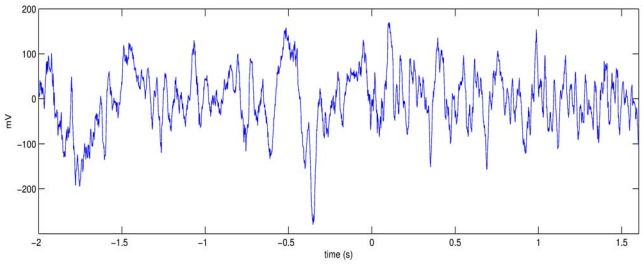

Fig. 4. A typical trial of LFP recording from area V1; t=0 represents stimulus onset.

IV. APPLICATION TO REAL NEURONAL SIGNALS

To illustrate the superiority of the improved SSA algorithm compared with EMD, we used LFP data from visual cortical area V1 of a macaque monkey maintaining stable fixation, while grating stimuli were presented away from fixation, in the receptive fields of recorded neurons. All procedures used for recording in the macaque monkey were in accordance with the European Directive on Animal Research, and approved by the animal research ethics committee (DEC) at the Radboud University Nijmegen. Here, we evaluated the ability of the two methods to identify high energy nonstationary gamma-band components, describing the relative enhancement of power within the gamma-band following visual stimulation. An example of a single-trial field potential recording is shown in Fig. 4 (time t=0 represents stimulus onset). Following a common procedure in neurobiology, several repeated trials were collected from the same macaque (n=63), and the corresponding LFPs recorded. The LFP recording from each trial was decomposed using the improved SSA algorithm and EMD. As proposed in [5], only the components with a dominant frequency in the gamma range [20,100] Hz (extended to avoid loss of information) were retained and exploited for signal reconstruction.

Fig. 5 shows the smoothed Hilbert spectra of both the EMD- and the SSA-reconstructed signal (Fig. 5-(a) and 5-(b), respectively) from the analysis of signal in Fig. 4 (the original Hilbert spectra were filtered with a 2-D moving average square window of size equal to 31 samples). The superiority of the improved SSA in tracking the relative enhancement in the gamma-band over the post-stimulus interval is clearly noticeable (Fig. 5-(b)).

Given the Hilbert spectrum of a signal $H(f,t)$, the spectral concentration of the gamma-band S_γ, around its main frequency peak f_c, on an interval $[t_1, t_2]$, with respect to the

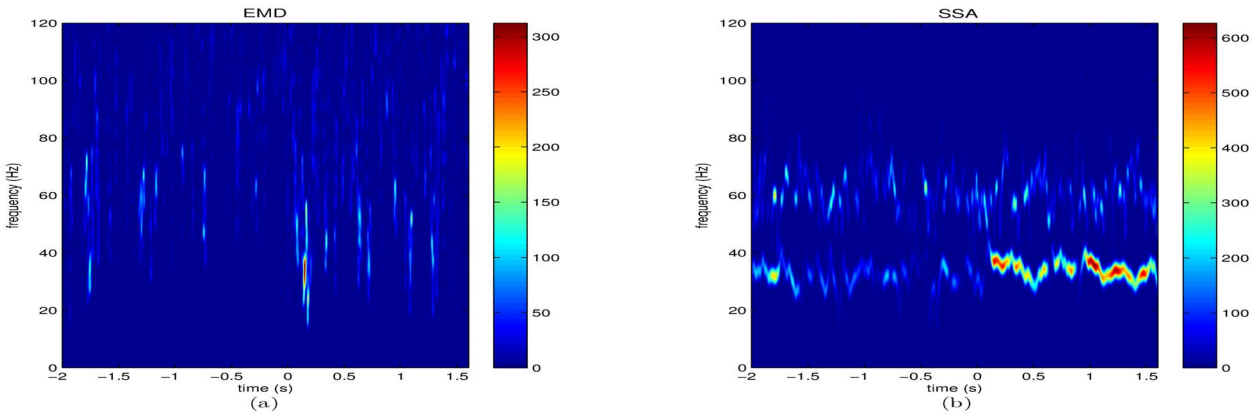

Fig. 5. Hilbert spectra of the (a) EMD-reconstructed signal and (b) SSA-reconstructed signal from signal in Fig. 4. Both signals have been reconstructed by exploiting only the components with a dominant frequency in the gamma-range [20,100] Hz.

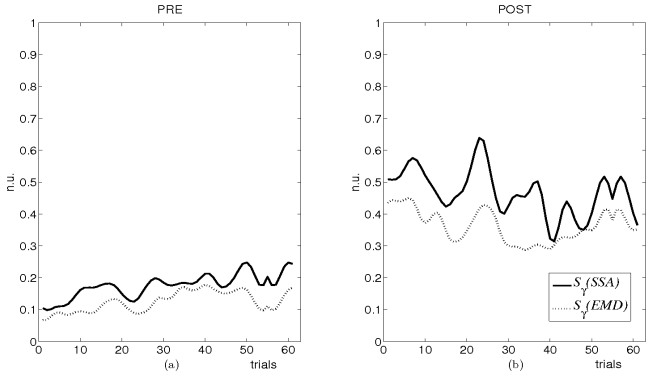

Fig. 6. Hilbert spectral concentration of the gamma-band, S_γ, computed on the EMD- and SSA-reconstructed signals (dotted and solid line, respectively) of the 62 trials for the (a) pre-stimulus interval and (b) post-stimulus interval; n.u.: normalized units.

total energy in the Hilbert spectrum, may be defined as:

$$S_\gamma = \frac{\int_{t_1}^{t_2}\int_{0.95f_c}^{1.05f_c} |H(f,t)|^2\, df\, dt}{\int_T \int_0^{F_S} |H(f,t)|^2\, df\, dt} \qquad (2)$$

such that the higher S_γ is the higher the gamma-frequency content of the analyzed signal is. T is the temporal length of the signal, and F_S its sampling frequency. S_γ was computed for each EMD- and SSA-reconstructed signal, from each trial, on two separated intervals: a pre-stimulus interval ($t < 0$), and one post stimulus ($t \geq 0$). The results for 62 trials are summarized in Fig. 6 (one trial was disregarded due to the strong influence of the trend on the provided components). On average, the higher energy content of the SSA compared with the EMD components was clear, particularly for the time interval starting after stimulus onset (paired Student's t-test: $p < 10^{-4}$).

Application of the improved SSA algorithm to LFPs from cortical visual area V1 showed to be able to resolve LFPs into sets of components having different degrees of oscillatory content. With respect to the energy content, SSA-components in the gamma-band frequency appear to be more meaningful than the intrinsic component provided by EMD, thus providing a better description of the enhancement generated by a visual fixation task. Hence, the improved SSA algorithm is a promising tool to analyze single-trial LFP recording to generate physiologically meaningful measurements of oscillatory neural behavior in the used model system. This promise needs to be put to the test in studies of functional connectivity among different brain areas, and also its theoretical validation needs further investigation.

REFERENCES

[1] A. Maier, G. K. Adams, C. Aura, and D. A. Leopold. Distinct superficial and deep laminar domains of activity in the visual cortex during rest and stimulation. *Front. in Sys. Neurosc.*, 4:1–11, 2010.

[2] P. Fries, J. H. Reynolds, A. E. Rorie, and R. Desimone. Modulation of oscillatory neuronal synchronization by selective visual attention. *Science*, 291(5508):1560–1563, February 2001.

[3] P. Fries. A mechanism for cognitive dynamics: neuronal communication through neuronal coherence. *Trends in Cognitive Sciences*, 9(10):474–80, 2005.

[4] M. Roberts, P. Fries, and P. De Weerd. The peak frequency of the gamma band shifts with stimulus contrast. In *FENS Forum*, 2010.

[5] H. Liang, S. L. Bressler, E. A. Buffalo, R. Desimone, and P. Fries. Empirical mode decomposition of field potentials from macaque V4 in visual spatial attention. *Biol. Cybern.*, 92:380–392, June 2005.

[6] N. E. Huang, Z. Shen, S. R. Long, M. C. Wu, H. H. Shih, Q. Zheng, N. C. Yen, C. C. Tung, and H. H. Liu. The empirical mode decomposition and the Hilbert spectrum for nonlinear and non-stationary time series analysis. *Proc. of the Royal Society of London. Series A: Mathematical, Physical and Eng. Sciences*, 454:903–995, 1998.

[7] Z. Peng, P. Tse, and F. Chu. An improved Hilbert-Huang transform and its application in vibration signal analysis. *Journal of Sound and Vibration*, 286(1-2):187–205, 2005.

[8] N. Golyandina, V. Nekrutkin, and A. A. Zhigljavsky. *Analysis of Time Series Structure: SSA and related techniques*. 2001.

[9] S. Aydın, H. Saraoğlu, and S. Kara. Singular Spectrum Analysis of Sleep EEG in Insomnia. *J. of Med. Systems*, 35:457–461, 2009.

[10] P. Celka and P. Colditz. A computer-aided detection of EEG seizures in infants: a singular-spectrum approach and performance comparison. *IEEE Trans. Biomed. Eng.*, 49(5):455–62, 2002.

[11] V. G. Moskvina and A. Zhigljavsky. An algorithm based on singular spectrum analysis for change-point detection. *Comm. in Stat. - Sim. and Comp.*, 32:319–352, 2003.

[12] P. Flandrin. Empirical Mode Decomposition. http://perso.ens-lyon.fr/patrick.flandrin/emd.html.